Tanaka, F., Yonekura, Y., Ikeda, A., Terada, K., Mikuni, N., Nishizawa, S., Ishizu, K., Okazawa, H., Hattori, N., Shibasaki, H., Konishi, J., Onishi, Y., 1997. Presurgical identification of epileptic foci with iodine-123 iomazenil SPET: comparison with brain perfusion SPET and FDG PET. Eur. J. Nucl. Med. 24, 27–34.

Umeoka, S., Matsuda, K., Baba, K., Usui, N., Tottori, T., Terada, K., Usui, K., Nakamura, F., Inoue, Y., Fujiwara, T., Mihara, T., 2007. Usefulness of ^{123}I-iomazenil single-photon emission computed tomography in discriminating between mesial and lateral temporal lobe epilepsy in patients in whom magnetic resonance imaging demonstrates normal findings. J. Neurosurg. 107, 352–363.

Van Bogaert, P., Massager, N., Tugendhaft, P., Wikler, D., Damhaut, P., Levivier, M., Brotchi, J., Goldman, S., 2000. Statistical parametric mapping of regional glucose metabolism in mesial temporal lobe epilepsy. Neuroimage 12, 129–138.

Wong, C.H., Bleasel, A., Wen, L., Eberl, S., Byth, K., Fulham, M., Somerville, E., Mohamed, A., 2010. The topography and significance of extratemporal hypometabolism in refractory mesial temporal lobe epilepsy examined by FDG-PET. Epilepsia 51, 1365–1373.

Please cite this article in press as: Hosomi, K., et al., Altered extrafocal iomazenil activity in mesial temporal lobe epilepsy. Epilepsy Res. (2012), http://dx.doi.org/10.1016/j.eplepsyres.2012.07.001

Electrocorticographic Control of a Prosthetic Arm in Paralyzed Patients

Takufumi Yanagisawa, MD, PhD,[1,2] Masayuki Hirata, MD, PhD,[1] Youichi Saitoh, MD, PhD,[1,5] Haruhiko Kishima, MD, PhD,[1] Kojiro Matsushita, PhD,[1] Tetsu Goto, MD, PhD,[1] Ryohei Fukuma, MS,[2,3] Hiroshi Yokoi, PhD,[4] Yukiyasu Kamitani, PhD,[2,3] and Toshiki Yoshimine, MD, PhD[1]

Objective: Paralyzed patients may benefit from restoration of movement afforded by prosthetics controlled by electrocorticography (ECoG). Although ECoG shows promising results in human volunteers, it is unclear whether ECoG signals recorded from chronically paralyzed patients provide sufficient motor information, and if they do, whether they can be applied to control a prosthetic.

Methods: We recorded ECoG signals from sensorimotor cortices of 12 patients while they executed or attempted to execute 3 to 5 simple hand and elbow movements. Sensorimotor function was severely impaired in 3 patients due to peripheral nervous system lesion or amputation, moderately impaired due to central nervous system lesions sparing the cortex in 4 patients, and normal in 5 patients. Time frequency and decoding analyses were performed with the patients' ECoG signals.

Results: In all patients, the high gamma power (80–150Hz) of the ECoG signals during movements was clearly responsive to movement types and provided the best information for classifying different movement types. The classification performance was significantly better than chance in all patients, although differences between ECoG power modulations during different movement types were significantly less in patients with severely impaired motor function. In the impaired patients, cortical representations tended to overlap each other. Finally, using the classification method in real time, a moderately impaired patient and 3 nonparalyzed patients successfully controlled a prosthetic arm.

Interpretation: ECoG signals appear useful for prosthetic arm control and may provide clinically feasible motor restoration for patients with paralysis but no injury of the sensorimotor cortex.

ANN NEUROL 2012;71:353–361

Paralyzed patients and amputees would benefit from cortically controlled prosthetics in the form of a brain–computer interface (BCI). Among the possible cortical signals available for BCI, electrocorticography (ECoG) offers one of the most clinically feasible options, having superior long-term stability and lower technical difficulty compared with other invasive signals.[1,2] Evidence from studies with nonparetic patients with epilepsy shows that some movements or movement intentions can be inferred from ECoG signals accurately enough to control external devices such as a computer cursor.[3–6] However, it is unclear whether these findings are applicable to paralyzed patients, whose sensorimotor cortices may have undergone extensive reorganization after deefferentation and deafferentation of the paralyzed body parts.

Paresis-associated cortical reorganization may modify ECoG signals of the sensorimotor cortex. Cortical reorganization occurs in the sensorimotor cortex of individuals with spinal cord injuries,[7–9] limb amputations,[10–12] and stroke.[13–15] Such cortical reorganizations have been shown to alter functional activations in the

View this article online at wileyonlinelibrary.com. DOI: 10.1002/ana.22613

Received Feb 4, 2011, and in revised form Aug 4, 2011. Accepted for publication Aug 12, 2011.

Address correspondence to Dr Hirata, Department of Neurosurgery, Osaka University Medical School, E6 2-2 Yamadaoka Suita, Osaka, Japan. E-mail: mhirata@nsurg.med.osaka-u.ac.jp or Dr Kamitani, ATR Computational Neuroscience Laboratories, 2-2-2 Hikaridai, Seika, Soraku, Kyoto 619-0288, Japan. E-mail: kmtn@atr.jp

[1]Department of Neurosurgery, Osaka University Medical School, Osaka; [2]ATR Computational Neuroscience Laboratories, Kyoto; [3]Nara Institute of Science and Technology, Nara; and [4]University of Tokyo Interfaculty Initiative in Information Studies Graduate School of Interdisciplinary Information Studies, Tokyo, Japan; [5]Department of Neuromodulation and Neurosurgery office for University-Industry Collaboration, Osaka, Japan.

Additional supporting information can be found in the online version of this article.

TABLE 1: Clinical Profiles

Patient No.	Age, yr/Sex	Diagnosis	Duration of Disease, yr	Paresis in Affected Limb (MMT)	Sensation in Affected Limb
N1	34/F	R intractable epilepsy	19	None	Normal
N2	14/M	R intractable epilepsy	7	None	Normal
N3	20/F	L intractable epilepsy	6	None	Normal
N4	22/F	R intractable epilepsy	10	None	Normal
N5	13/M	L intractable epilepsy	11	None	Normal
P1	49/M	R putaminal hemorrhage	2	Slightly spastic (5−)	Hypoesthesia
P2	66/F	R subcortical infarction	3.3	Spastic (4)	Hypoesthesia
P3	64/M	R thalamic hemorrhage	7	Spastic (4)	Hypoesthesia
P4	65/M	Ruptured spinal dAVF	8	Spastic (4)	Hypoesthesia
S1	31/M	L brachial plexus avulsion	5	Complete (0)[a]	Anesthesia
S2	49/M	L brachial plexus avulsion	6	Severe (1)[a]	Severe hypoesthesia
S3	47/M	Amputation below L shoulder	3.3	No arm	None

[a]Post transplantation of intercostal nerve.
dAVF = dural arteriovenous fistula; F = female; L = left; M = male; MMT = manual muscle test; R = right.

cortices and affect motor function,[14] sensation, and recognition of body parts.[10,11,16] However, quantitative data are lacking on altered functional activations of the sensorimotor cortex after cortical reorganization and subsequent modification of ECoG signals.

We examined ECoG signals of nonparalyzed patients and patients with different levels of motor dysfunctions to quantitatively address 3 questions: (1) Do the ECoG signals of patients with chronic motor dysfunctions show preservation of spatiotemporal patterns of activation even after reorganization? (2) How much are ECoG activation maps for different motor tasks modified in the reorganized sensorimotor cortex? and (3) Can ECoG activation be applicable to controlling a prosthetic arm?

Patients and Methods

Patient Population

Twelve patients (4 female, 8 male; age range, 13–66 years) with subdural electrodes participated in this study. The patients had different degrees of motor dysfunctions and sensory disturbances (Table 1). Five patients (N1–N5) with epilepsy had no motor dysfunctions; 4 patients (P1–P4) had spastic paresis and weakness in their upper limbs due to strokes without damage to the sensorimotor cortex (moderate motor dysfunction); and 3 patients (S1–S3) had severely impaired sensorimotor function of their limbs due to brachial plexus root avulsion or amputation (severe motor dysfunction; Supplementary Methods). Patients S1–S3 differed in their ability to imagine movement of their affected limbs (Table 2). All participants or their guardians gave written informed consent to participate in the study, which was approved by the ethics committee of Osaka University Hospital.

All patients had been implanted with subdural electrode arrays that covered a broad sensorimotor cortical area, including the hand motor strip. These arrays were kept in place for 2 weeks to determine either the epileptic foci or the optimal stimulation sites to achieve maximum pain reduction.[17] At the end of these 2 weeks, the arrays were removed. In impaired patients, 4 permanent electrodes were then placed at the sites where stimulation provided optimal pain control.

Movement Tasks

Experiments were performed in an electromagnetically shielded room approximately 1 week after electrode placement. The first session was designed to train the decoder on the ECoG signals (decoder training session). Patients performed 1 of 3 possible movement tasks that differed by the set of movement types that were executed: (1) grasping, thumb flexion, and elbow flexion (P1, P2, S1–S3); (2) grasping, pinching, hand-opening, elbow flexion, and tongue protrusion (P3); or (3) grasping, pinching, hand-opening, elbow flexion, and elbow extension (N1–N5, P4). For movement task 3, the patients were first instructed to perform the 3 hand movements. Then, after a free-run session in which patients undertook movements at their own pace, if they were able to undertake additional sessions without fatigue, they were instructed to perform 5 movements, preferably ones involving the elbow. Grasping and elbow flexion were commonly performed among all patients, although we selected the

TABLE 2: Summary of the Decoding Results

Patient No.	Ability to Imagine Movements	% Correct (grasp vs elbow)	Mean ± SD	% Correct (move vs rest)	Mean ± SD
N1		92.9	92.5 ± 3.4 ($p < 0.05$)	96.6	93.6 ± 4.4 (NS)
N2		98.2		94.5	
N3		90.7		86.0	
N4		90.5		94.2	
N5		90.0		96.4	
P1		86.7	89.2 ± 5.8 (NS)	95.7	95.6 ± 4.5 (NS)
P2		85.7		100.0	
P3		97.9		89.5	
P4		86.7		97.3	
S1	Easy	90.3	71.3 ± 17.0 ($p < 0.05$)	98.2	93.2 ± 4.6 (NS)
S2	Slightly difficult	57.3		92.2	
S3	Difficult	66.3		89.2	

NS = not significant; SD = standard deviation.

3 types of movement tasks to adjust the way patients could control the prosthesis.

The patients selected and performed one of the movements within a presented task after being cued with auditory beeps (Fig 1A). The patients were instructed to execute movements immediately after the third beep and then return their hands or elbows to a resting position. For the resting position, patients were instructed to relax their hands or elbows with slightly flexed joints. Each type of movement was performed approximately 30 to 100 times. Patients S1–S3 were instructed to attempt the movements of their affected limbs immediately after the auditory cue. The movement instructions were delivered using a PC monitor controlled by ViSaGe (Cambridge Research System, Rochester, UK) placed in front of the patients. The decoder training session was open loop. The patients were not informed of the classifier results and therefore did not have an opportunity for learning or improving their performance.

After the decoder training session, 4 patients repeated the same task they had performed during the session, but at self-paced intervals without external cues (free-run session, see Fig 1B). These patients had recently performed the task and were able to continue without extensive fatigue. Without receiving further training, they were instructed to control the prosthetic arm by performing their hand and elbow movements. Patient N1 could not control the elbow of the prosthetic arm due to mechanical problems of the prosthesis.

ECoG Recording and Preprocessing

For each patient, 15 to 60 planar-surface platinum grid electrodes were placed over the sensorimotor cortex and within the central sulcus (intrasulcal electrodes)[18] (see Supplementary Methods). Video recording and electromyographic (EMG electrode; Nihon Koden, Tokyo, Japan) recordings of their hands and arms were performed solely to identify the performed movements.

ECoGs were recorded and digitized at a sampling rate of 1,000Hz. During the decoder training session, the ECoG signals were obtained time-locked to the cue signal. In the free-run session, 1-second duration ECoG signals were recorded online at 200-millisecond intervals. A fast Fourier transformation (FFT; EEGLAB v5.03) was performed for each 1-second signal to obtain the power of each of the 3 frequency bands (2–8, 8–25, and 80–150Hz) for each electrode. We used FFT to complete the online decoding over the 200 milliseconds. The 3 frequency bands were chosen based on our previous studies.[19]

Decoding Algorithms and Prosthetic Hand Control

To infer, or decode, the movement types executed or attempted by the patients, we constructed a linear classifier trained by a linear support vector machine, the SVM decoder (see Supplementary Methods).[18,20,21] The trained SVM decoder was inputted with the ECoG signals to output an inferred movement type. A 5-fold cross-validation was used to test how well the decoder could generalize.

To apply the SVM decoder to the free-run sessions without external cues, we developed another decoder (GPR decoder; see Supplementary Methods). The trained GPR decoder was also inputted with the ECoG signals to output an estimated

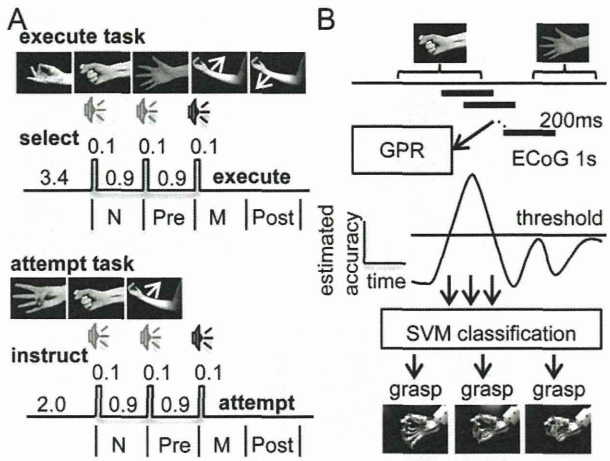

FIGURE 1: Task paradigm. (A) The task paradigm during the decoder training session. In the execute task, patients selected and executed 1 of 3 (or 5) movements after the sound cue. The cue consisted of 3 beeps 1 second apart that recurred every 5.5 seconds. The movements were performed with the arm contralateral to the implanted electrodes. In the attempt task, patients were instructed which of the 3 (or 5) movements to attempt. The 1-second electrocorticography (ECoG) signals used for the decoding analysis are shown below the time line: N = used for normalization and resting state; Pre = used as the first period by the Gaussian process regression (GPR) decoder; M = used as the move state; Post = as the last period by the GPR decoder. (B) Controlling the prosthetic hand with 2 decoders. The GPR decoder estimated the accuracy of the time determined to be necessary for the support vector machine (SVM) decoder to classify the ECoG signals. The prosthetic hand was controlled incrementally according to the decoding results.

classification accuracy of the SVM decoder. When the estimated classification accuracy exceeded a certain threshold value (see Fig 1B), the SVM decoder classified the ECoG signals to infer the intended movement (Supplementary Fig 3).

The GPR decoder was trained using a Gaussian process regression (GPR),[22] which is one kind of Bayesian approach.[23] We used GPR because it could be applied to the nonlinear data with a simple model. The GPR decoder was trained with the classification accuracies and the 3 frequency band powers of 3 time domains (Pre, M, and Post in Fig 1A; see Supplementary Methods). The classification accuracies were evaluated by the mutual information, which quantified the confusion matrix resulting from the SVM decoder. The mutual information was normalized by using the values of the 3 time domains. The trained GPR decoder estimated the classification accuracy with 3 frequency band powers at a given time in a free-run session. The GPR and SVM decoders were trained for hand and elbow movements separately.

The commands to the prosthetic arm were updated by the host computer system every 200 milliseconds. When the SVM decoder inferred a movement type, the posture of the prosthetic arm was partially altered to match the posture of the inferred movement (see Supplementary Methods). Completing a movement required 2 or 3 consecutive matched decodings. This incremental control of the prosthetic hand permitted the desired posture even when the classification performance of the SVM decoder was not perfect; the classification errors of the

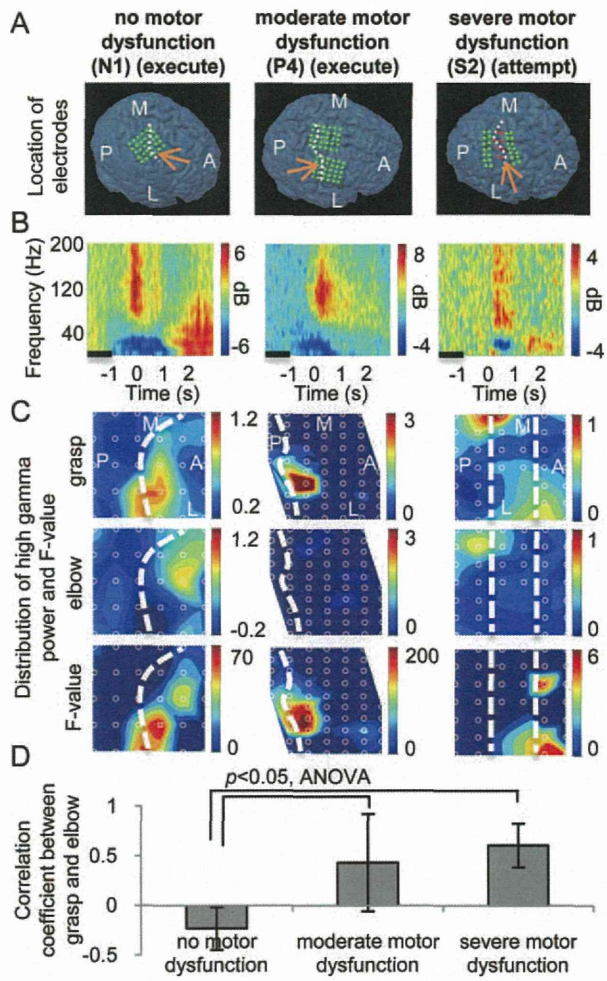

FIGURE 2: Representative results of time-frequency analysis. (A) Locations of implanted electrodes for patients N1, P4, and S2 are indicated by the green (implanted on the brain surface) and red (implanted within the central sulcus) filled circles on the 3-dimensional brain renderings of magnetic resonance imaging volumes. The dashed white line indicates the location of the central sulcus. Only the electrodes used for the analysis are shown. (B) Power spectra of the electrocorticographic signals recorded during grasping (execute) or attempt to grasp from the electrodes on the primary motor cortex indicated by the orange arrows in A. The black horizontal bars show the 1,000-millisecond period used for normalization. Time 0 corresponds to the onset cue. (C) The high gamma power is color coded to the location of the electrodes for grasping and elbow flexion. The direction indicators correspond to A = anterior, P = posterior, M = medial, and L = lateral on the brain. The white dashed lines and the white circles indicate the locations of the central sulcus and the electrodes, respectively. For the patient S2, the electrodes between the 2 white lines were located within the central sulcus (intrasulcal electrodes; see Supplementary Methods). The lowest figure of each patient shows the distribution of the *F* value with statistical significance ($p < 0.05$). (D) The correlation coefficient of the high gamma powers between hand grasping and elbow flexion for each patient's group. ANOVA = analysis of variance.

decoder caused only a tremor of the prosthetic arm as it moved to the desired posture.

Offline Analyses

The ECoG signals of grasping and elbow flexion were compared among patients. A Hilbert transformation (EEGLAB v5.03) was used to obtain the temporal power spectral density of each frequency band (see Supplementary Methods). The temporal powers were normalized by powers of the initial 1-second period (−2 to −1 seconds) of each trial.

The variability of the high gamma power of 0 to 1 second was statistically evaluated among 2 types of movements by the F value of one-way analysis of variance (ANOVA) for each electrode. The statistical similarity of the high gamma power maps was evaluated by determining the correlation coefficient of the mean power maps of 2 movements. The classification accuracies for inferring 2 movements using the SVM decoder with the high gamma powers were compared among patients.

Results

Time-Frequency Analysis

The power spectrum of the ECoG signals showed some characteristic modulations among patients. Figure 2B illustrates examples of the power spectrum time-locked to the external cues while grasping or attempting to grasp. An increase in the high gamma power and decreases in the alpha and beta powers were consistently observed for all patients with different levels of motor dysfunctions. The spatial distributions of the high gamma power during movement (0–1 second) were obviously different for each movement (see Fig 2C), and the ANOVA F value revealed that high gamma powers were significantly modulated between the movements. Notably, the powers around the central sulcus showed significant differences ($p < 0.05$). The characteristic modulations of the high gamma power were consistently observed among all patients, although the F values pertaining to variability were lower in patients with severe dysfunctions than in other patients. Moreover, the correlation coefficient of the spatial distribution of the high gamma power between the movements was significantly high for the patients with motor dysfunctions (see Fig 2D).

Decoding Analysis

The accuracy of classifying (ie, decoding) the movements was compared among the frequency band powers at each time. Figure 3 shows the color-coded percentage of correct movement classifications averaged over each patient group. Regardless of the level of motor dysfunctions, the 2 movement types were best inferred by using the high gamma power around the movement onset.

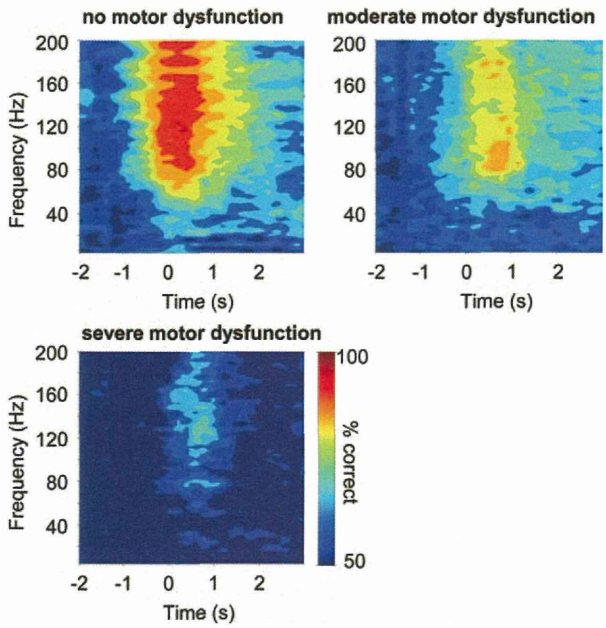

FIGURE 3: Averaged classification accuracy with each frequency band power. Classification accuracies with each frequency band power were averaged for the patients of each group and color coded at the center of each frequency band and time domain. Time 0 corresponds to the sound cue for the movements.

The movement classifications were carried out for all patients with a high gamma power for 0 to 1 seconds. The classification accuracy of patients S1 to S3 was significantly inferior to that of patients N1 to N5 (ANOVA, $p < 0.05$; see Table 2). However, these accuracies were still above levels that would occur by chance (50%). This relationship was also observed in the classification of 3 types of movements (Supplementary Table). On the other hand, the accuracies to classify the resting state (−2 to −1 seconds) and the movement state (0 to 1 seconds) were not significantly different among the 3 patient groups (see Table 2).

Decoding in Free-Run and Real-Time Control of a Prosthetic Hand

The classification accuracy of 3 hand movements with the SVM decoder varied with time in the decoder training session (Fig 4B). It was highest immediately after the onset cues (eg, when the hand EMG response started to increase; see Fig 4A). The trained GPR decoder accurately inferred the timing of the peak and zero value of the normalized mutual information only using the 3 frequency bands at each time (see Fig 4C).

Using the trained decoders, the ECoG signals were decoded in real time while the patient, without further training, voluntarily (ie, without cue) performed the 3 to 5 types of movements (free-run period, see Fig 4D). The estimated mutual information peaked when the standard

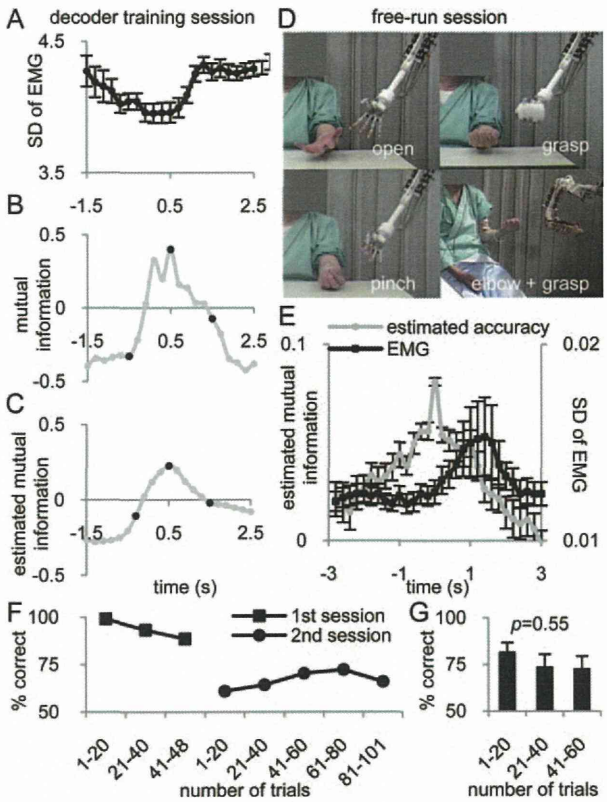

FIGURE 4: Prosthetic control with the electrocorticography (ECoG) signals. (A) The standard deviations (SDs) of the electromyographic (EMG) responses averaged over 1-second periods are shown at each time centered on the onset cue (0). (B) For patient P4, the mutual information for the performed movements and the inferred movements was normalized at each time. The values of the mutual information at 3 time domains (black circle) trained the Gaussian process regression (GPR) decoder. (C) The mutual information estimated by the trained GPR decoder at each time. (D) Representative photographs of the prosthetic arm controlled in real time by the ECoG signals of patient P4. (E) The estimated mutual information and standard deviation of the EMG responses were averaged for the 6 seconds time-locked to the peak values of the estimated mutual information that exceeded a value of 0.07. (F) The percentage correct of each 20 trials over the course of the entire free-run session of P4 (squares = first session; circles = second session). (G) The percentage correct of each 20 trials were not significantly different among all sessions of 4 patients (analysis of variance, $p = 0.55$).

deviation of the EMG response started to increase, indicating that the GPR decoder successfully decoded the movement onset in the free-run session (see Fig 4E).

The prosthetic arm was controlled in real time according to the decoding results of the SVM and GPR decoders, mimicking the hand movements of patients. The prosthetic hand completed the same movement of patient P4 in 42 of 48 attempts (87.5%; Supplementary Video 1). Each hand movement required an average of 2.2 incremental movements of 4.2 seconds each. By voluntarily moving his own hand, patient P4 was able to catch and hold an object for seconds and intentionally release the object from the prosthetic hand (Supplementary Video 2). Moreover 4 days after the first experiments (second free run), the patient was still able to perform the same free-run task (Table 3, see Fig 4F, Supplementary Video 3), using the decoder trained in those initial experiments. The 3 other participating patients (N1, N3, N4) were also able to voluntarily control the prosthetic arm (see Table 3). Notably, the classification accuracy of the SVM decoder was not significantly different between the training session and the free-run session (ANOVA, $p = 0.06$) and over the course of the each free-run session (ANOVA, $p = 0.55$; see Fig 4F, G). Finally, the elbow of the prosthetic arm was simultaneously controlled by the other GPR decoder for the elbow (Supplementary Video 4). The success rate for complete elbow movements of the prosthetic arm was significantly lower than that of the training (ANOVA, $p < 0.05$).

Patient N1 described her impression of control as thinking at first that the prosthetic arm moved in mimicry of her movements, rather than that she was controlling the prosthesis. But at the end of the experiment, she realized she was able to control the prosthesis well. However, no patient controlling the prosthesis stopped moving their own limb.

Discussion

We have shown that ECoG signals recorded from patients with chronic motor dysfunctions still represented motor information via high gamma power to a degree that they could be decoded successfully enough to control a prosthetic hand. However, the modulation of the representation for different movements may have deteriorated depending on the degree of impairment. Our quantitative evaluation of motor representations in the reorganized cortex elucidated pathological states of patients with motor dysfunctions and demonstrated the applicability of these representations for an ECoG-based BCI to improve patients' quality of life.

Preserved Features following Cortical Reorganization

The spatiotemporal features of the ECoG signals during movements or attempts at movements were qualitatively preserved in the sensorimotor cortex of impaired patients. During movements, high gamma power was consistently increased around the central sulcus, even for severely impaired patients. This is consistent with previous functional magnetic resonance imaging (fMRI) studies showing that activation of the motor cortex is

TABLE 3: Summary of the Real-Time Control of the Prosthetic Hand

Patient No. and Session		Hand Movements (grasp, pinch, open)				Elbow Movements (flexion, extension)			
		% Correct of Training	% Correct to Complete (correct/trial)	% Correct of SVM Decoder in Free Run	Time/Count to Complete (s/count)	% Correct of Training	% Correct to Complete (correct/trial)	% Correct of SVM Decoder in Free Run	Time/Count to Complete (s/count)
N1	1st	79.2	71.2 (37/52)	76.1	1.8/3.3	64.3	—	—	—
	2nd		51.2 (22/43)	67.0	1.5/3.3				
N3	1st	70.0	85.7 (30/35)	80.7	1.6/3.3	77.5	14.3 (1/7)	87.5	13.6/3
	2nd		47.2 (17/36)	81.0	1.3/2.7				
N4	1st	60.8	64.7 (11/17)	70.3	1.3/3.7	74.0	33.3 (1/3)	60.0	3.3/2
	2nd		—	—	—				
P4	1st	80.8	87.5 (42/48)	68.8	2.2/4.2	70.0	54.2 (26/48)	90.1	2.3/3.7
	2nd		62.3 (63/101)	62.3	2.0/4.1				
Mean ± SD		72.7 ± 9.2	77.3 ± 11.1	74.0 ± 5.5	1.7 ± 0.4/ 3.6 ± 0.4	71.5 ± 5.7	33.9 ± 20.0 ($p < 0.05$, ANOVA)	79.2 ± 16.7	6.4 ± .6.3/ 2.9 ± 0.9
			53.6 ± 7.8	70.1 ± 9.7	1.6 ± 0.4/ 3.6 ± 0.7				

ANOVA = analysis of variance; SVM = support vector machine.

preserved even in paralyzed patients,[24–26] because the high gamma activity is correlated with the fMRI blood oxygen level-dependent signal.[27]

The decoding analysis showed that modulation of the high gamma power provided the most information about the movement types. This result was consistent with previous studies that showed human movements could be inferred by using ECoGs.[3,4,28,29] It was suggested that the basic features of cortical processing with high gamma powers are preserved following cortical reorganization resulting from motor dysfunctions.

Deteriorated Motor Representation Accompanying Phantom Limb Pain

The decreased decoding accuracy in patients with motor dysfunctions indicated that the high gamma powers were not prominently modulated among the different types of movements, suggesting that modulation of the high gamma power (ie, motor representation) had significantly deteriorated following cortical reorganization. Conversely, the increased correlation of the high gamma powers between different movements suggested that the representations of the movements became similar to each other in the impaired patients. Notably, this similarity was not due to a weakened representation; an increase in the high gamma power during movement was accurately decoded even in the patients with severe dysfunctions. Our results suggested that the modulation of the high gamma powers had deteriorated in the impaired patients with increased similarity of the power maps among movements. This result was consistent with previous reports showing that cortical representations of nonaffected body parts shifted to overlap representations of affected body parts in phantom limb pain patients.[11,16,30] It was suggested that the decreased decoding accuracy of movement types might be due to overlaps in the spatial distributions of the high gamma powers for each movement.

Our data also suggested that the deteriorated modulation of motor representations in patients S1 to S3 was related to patients' ability to imagine movements. Classification accuracy of these patients was highest for the patient who could most easily imagine the movements and lowest for the patients who could hardly imagine movements. This relation was also observed in the distribution of the F values of the high gamma powers (Supplementary Fig 4). For some patients who lost the ability to imagine intentionally moving their phantom limbs, the motor representation, or high gamma powers, may no longer be modulated well enough to be decoded. We suggest that cortical reorganization did not alter the characteristic features of the ECoG signals, but rather affected modulation of the representation, related to the ability to imagine the movements.

Prosthetic Hand Control Applied to a Diverse Patient Population

Successful control of the prosthetic arm was demonstrated with the SVM and GPR decoders, which accurately inferred various movement types from the ECoG signals of patients with motor dysfunctions. This suggests the feasibility of restoring purposeful movement based on a BCI. Although the cortical control of some prostheses has already been demonstrated with other invasive signals,[31,32] our success with the ECoG signals may be beneficial for clinical applications because an ECoG-based BCI has advantages in signal stability and durability that are absolutely necessary for clinical application.[2] As we demonstrated, the prosthetic hand could be controlled for several days with a single decoder trained once at the first session. This reveals the robustness of our decoding method and the stability of the ECoG signals. Moreover, our method was demonstrated with an elderly patient who was able to successfully and naturally control the prosthetic arm without any prior training. A requisite for a clinically useful BCI system is that it be developed to be stably and easily used by a diverse population of patients in their daily lives.

Acknowledgments

This work was supported in part by the Strategic Research Program for Brain Sciences of Ministry of Education, Culture, Sports, Science and Technology-Japan (MEXT); KAKENHI (22700435); Nissan Science Foundation; Ministry of Health, Labor, and Welfare (18261201); and Strategic Information and Communications R&D promotion Programme (SCOPE), SOUMU.

Potential Conflicts of Interest

Nothing to report.

References

1. Leuthardt EC, Schalk G, Moran D, et al. The emerging world of motor neuroprosthetics: a neurosurgical perspective. Neurosurgery 2006;59:1–14.
2. Chao ZC, Nagasaka Y, Fujii N. Long-term asynchronous decoding of arm motion using electrocorticographic signals in monkeys. Front Neuroeng 2010;3:3.
3. Pistohl T, Ball T, Schulze-Bonhage A, et al. Prediction of arm movement trajectories from ECoG-recordings in humans. J Neurosci Methods 2008;167:105–114.
4. Schalk G, Miller KJ, Anderson NR, et al. Two-dimensional movement control using electrocorticographic signals in humans. J Neural Eng 2008;5:75–84.
5. Schalk G, Kubanek J, Miller KJ, et al. Two-dimensional movement trajectories using electrocorticographic signals in humans. J Neural Eng 2007;4:264–275.

6. Miller KJ, Zanos S, Fetz EE, et al. Decoupling the cortical power spectrum reveals real-time representation of individual finger movements in humans. J Neurosci 2009;29:3132–3137.
7. Bruehlmeier M, Dietz V, Leenders KL, et al. How does the human brain deal with a spinal cord injury? Eur J Neurosci 1998;10: 3918–3922.
8. Green JB, Sora E, Bialy Y, et al. Cortical motor reorganization after paraplegia: an EEG study. Neurology 1999;53:736–743.
9. Mikulis DJ, Jurkiewicz MT, McIlroy WE, et al. Adaptation in the motor cortex following cervical spinal cord injury. Neurology 2002;58:794–801.
10. Ramachandran VS, Rogers-Ramachandran D, Stewart M. Perceptual correlates of massive cortical reorganization. Science 1992; 258:1159–1160.
11. Flor H. Phantom-limb pain: characteristics, causes, and treatment. Lancet Neurol 2002;1:182–189.
12. Roricht S, Meyer BU, Niehaus L, et al. Long-term reorganization of motor cortex outputs after arm amputation. Neurology 1999;53:106–111.
13. Green JB. Brain reorganization after stroke. Top Stroke Rehabil 2003;10:1–20.
14. Nudo RJ, Wise BM, SiFuentes F, et al. Neural substrates for the effects of rehabilitative training on motor recovery after ischemic infarct. Science 1996;272:1791–1794.
15. Gerloff C, Bushara K, Sailer A, et al. Multimodal imaging of brain reorganization in motor areas of the contralesional hemisphere of well recovered patients after capsular stroke. Brain 2006;129:791–808.
16. Flor H, Elbert T, Knecht S, et al. Phantom-limb pain as a perceptual correlate of cortical reorganization following arm amputation. Nature 1995;375:482–484.
17. Hosomi K, Saitoh Y, Kishima H, et al. Electrical stimulation of primary motor cortex within the central sulcus for intractable neuropathic pain. Clin Neurophysiol 2008;119:993–1001.
18. Yanagisawa T, Hirata M, Saitoh Y, et al. Neural decoding using gyral and intrasulcal electrocorticograms. Neuroimage 2009;45:1099–1106.
19. Yanagisawa T, Hirata M, Saitoh Y, et al. Real-time control of a prosthetic hand using human electrocorticography signals. J Neurosurg 2011;114:1715–1722.
20. Kamitani Y, Tong F. Decoding the visual and subjective contents of the human brain. Nat Neurosci 2005;8:679–685.
21. Kamitani Y. Brain decoder toolbox. 2010. Available at: http://www.cns.atr.jp/dni/en/downloads/brain-decoder-toolbox. Assessed on 12 May 2010.
22. Ebden M. Gaussian processes for regression: a quick introduction. Available at: http://www.robots.ox.ac.uk/~mebden/reports/GPtutorial.pdf. Assessed on 15 December 2010
23. Rasmussen C, Williams C. Gaussian processes for machine learning. Cambridge, MA: MIT Press, 2006.
24. Shoham S, Halgren E, Maynard EM, et al. Motor-cortical activity in tetraplegics. Nature 2001;413:793.
25. Corbetta M, Burton H, Sinclair RJ, et al. Functional reorganization and stability of somatosensory-motor cortical topography in a tetraplegic subject with late recovery. Proc Natl Acad Sci USA 2002; 99:17066–17071.
26. Cramer SC, Lastra L, Lacourse MG, et al. Brain motor system function after chronic, complete spinal cord injury. Brain 2005;128: 2941–2950.
27. Logothetis NK, Pauls J, Augath M, et al. Neurophysiological investigation of the basis of the fMRI signal. Nature 2001;412: 150–157.
28. Kubanek J, Miller KJ, Ojemann JG, et al. Decoding flexion of individual fingers using electrocorticographic signals in humans. J Neural Eng 2009;6:1–14.
29. Crone NE, Sinai A, Korzeniewska A. High-frequency gamma oscillations and human brain mapping with electrocorticography. Prog Brain Res 2006;159:275–295.
30. Karl A, Birbaumer N, Lutzengerger W, et al. Reorganization of motor and somatosensory cortex in upper extremity amputees with phantom limb pain. J Neurosci 2001;21:3609–3618.
31. Velliste M, Perel S, Spalding MC, et al. Cortical control of a prosthetic arm for self-feeding. Nature 2008;453:1098–1101.
32. Hochberg LR, Serruya MD, Friehs GM, et al. Neuronal ensemble control of prosthetic devices by a human with tetraplegia. Nature 2006;442:164–171.

Smart electrode array device with CMOS multi-chip architecture for neural interface

T. Noda, K. Sasagawa, T. Tokuda, Y. Terasawa, H. Tashiro, H. Kanda, T. Fujikado and J. Ohta

A CMOS integrated flexible neural interface device has been designed and fabricated. The device enables electrical stimulation of neural tissues using an array of smart electrodes. The smart electrodes have versatile functions owing to the use of a dedicated CMOS microchip. These multiple smart electrodes also provide the array with sophisticated functions with only four wiring connections to external equipment. Moreover, the multi-chip architecture of the device is highly flexible and has low invasiveness to living body tissue. An *in vivo* evaluation of retinal stimulation was performed after implanting the device in the eye of an experimental animal. The stimulus function of the device was successfully demonstrated by observing responses in the visual cortex caused by the stimulation.

Introduction: Flexible electrode array devices for *in vivo* or *in vitro* research and medicine have been developed and utilised [1, 2]. The typical configuration of such a device consists of metal electrodes on a flexible substrate. The electrodes are directly wired to external equipment. Such devices can easily cover a large area and they have low invasiveness. However, increasing the number of electrodes results in a huge number of wirings, which makes using a large number of electrodes difficult in some applications.

Another area that has been the subject of much research is CMOS technology- or MEMS technology-based neural interface devices that include brain–machine interface (BMI) devices [3, 4]. These devices have many advantages that are obtained by using the high-level functions of CMOS circuitry and/or microfabrication with MEMS technology. However, some intrinsic problems result from the utilisation of CMOS or MEMS technology. These devices are much harder than living body tissue. Affinity to the tissue is not necessarily high, so reduced invasiveness is desired. Moreover, it is not realistic to cover a large area on a square-centimetre scale with the devices.

We previously proposed a multi-chip architecture to realise a CMOS-based flexible retinal stimulator [5, 6]. The multi-chip architecture makes it possible to achieve both multi-point stimulation of a large area and flexibility. In this reported study, a flexible neural interface device was proposed and fabricated. The device has an electrode array that is smart owing to the CMOS microchip. Functional validation was also performed with the device.

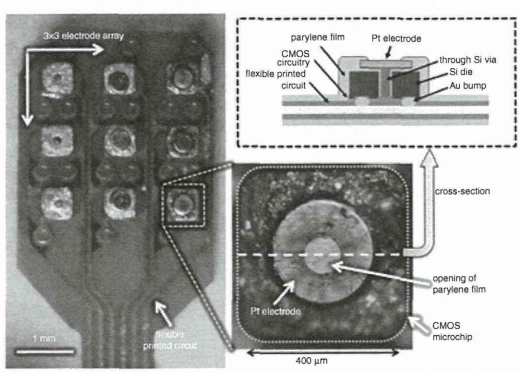

Fig. 1 *Photographs of fabricated device with CMOS smart electrodes.*
Inset: cross-sectional structure of device

Fabrication of device: Fig. 1 shows the fabricated flexible neural interface device with CMOS-based smart electrodes. The device has a multi-chip architecture. A flexible printed circuit (FPC) made of polyimide was used as a substrate because it can be used as both a supporter of the CMOS microchips and the wiring. On the substrate, nine CMOS microchips were mounted in a 3 × 3 array using flip-chip bonding technology. The die size of each microchip is 400 μm square, and the flexible substrate is exposed only at the gaps between adjacent microchips. Thus, the device can flex easily and smoothly. Operational control circuits were integrated into the microchip. Thanks to the CMOS circuits, only four wirings exist on the device, and they are connected to external equipment. All of the CMOS microchips have stimulus electrodes on the backside. Each electrode site on the electrode array consists of the pair of a CMOS microchip and its back electrode. The CMOS circuitries are electrically connected to the electrodes by through-silicon vias.

The electrodes are utilised for neural stimulation and measurement. CMOS circuitries for stimulation and measurement were also integrated into the microchips. CMOS-based smart electrodes operate actively unlike traditional passive electrodes without microchips.

A dedicated CMOS chip was designed and fabricated using the standard 0.35 μm CMOS process and is shown in Fig. 2*a*. The chip consists of a current generator for neural stimulation and operational control logic circuitry that controls the operation of all microchips mounted on the device. Each microchip mounted on the stimulator has an intrinsic ID. A target microchip can be selected using the ID number, and the operation parameters can be configured. The output strength of a stimulus current generator can be controlled with a control command signal from 50 to 1000 μA with 50 μA steps. Both monophasic and biphasic constant current pulses can be generated. A neural activity measurement function is also integrated in the design.

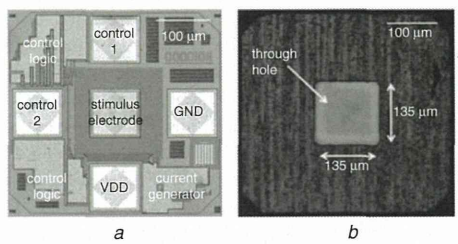

Fig. 2 *Micrographs of fabricated CMOS microchip*
a Front (circuitry) side
b Backside

The through-silicon via was formed in a post-CMOS process. Through-silicon deep reactive ion etching (deep RIE) with a Bosch process was performed. A 135 μm square through-hole was formed at the centre of the microchip, as shown in Fig. 2*b*. An I/O pad for a stimulus electrode can be connected electrically from the backside of the microchip.

Through-hole formed microchips were then mounted on the FPC. Flip-chip bonding technology was utilised in this process with Au stud bumps and anisotropic conductive paste. After the flip-chip bonding process, a parylene layer was formed to prevent short-circuits between the bulk silicon and conductive epoxy resin filled in the through holes. Before curing the conductive epoxy resin, Pt electrodes 250 μm in diameter were placed onto the through hole, and then the resin was cured. The entire FPC with microchips and electrodes was coated with 5 μm-thick parylene-C. As a final process, the parylene film on the Pt electrode was removed by laser processing. The exposed area of the Pt electrode was about 200 μm in diameter.

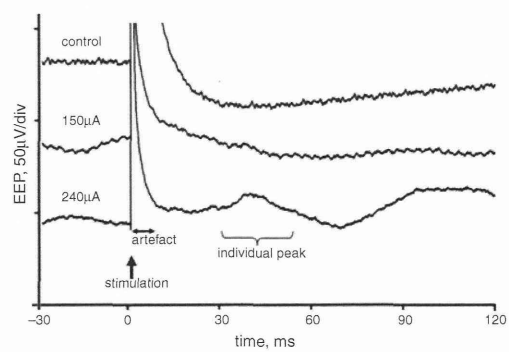

Fig. 3 *Electrically evoked potential response with anodic pulse stimulation of retinal cells.*
Post-sacrifice potential responses as control data are also plotted

Animal experiments: We validated the functioning of the fabricated device by conducting a retinal stimulation of a rabbit. The fabricated device and a counter electrode were implanted into the eyeball of an anaesthetised rabbit. Current-controlled retinal stimulations were performed in a suprachoroidal transretinal stimulation (STS) configuration [7, 8]. Responses of retinal stimulation can be observed through brain

waves. A screw electrode was placed onto the visual cortex of the rabbit brain for observation of electrically evoked potentials (EEPs).

One site of the 3 × 3-electrode array was selected, and the stimulus current generator was programmed into anodic pulse mode using control commands. We stimulated the retina while varying the intensity of the stimulus current pulse at a pulse width of 1 ms and a repetition cycle of 2 s. Fig. 3 shows the measured EEP responses. A large peak around 0 ms is an artefact caused by the stimulations. If a retinal cell is sufficiently stimulated, an individual peak of EEP is obtained after 30–50 ms following the stimulation. An individual peak was observed with a 240 μA pulse current. However, 150 μA pulse stimulation was not enough to evoke retinal cells. These results successfully demonstrate the electrical stimulation function of the device.

Conclusions: A CMOS-based smart electrode array is proposed in this Letter. The device not only has multi-functions owing to the use of a CMOS microchip but also flexibility that is obtained with the multi-chip architecture. Operational control circuits and a stimulus current generator were integrated into a dedicated CMOS microchip. The microchips were flip-chip mounted onto a flexible printed circuit. Pt disc electrodes were mounted onto the back side of the microchip and connected electrically by a through-silicon via. The completed device was evaluated through an *in vivo* experiment. The fabricated device was implanted into the eyeball of a rabbit, and retinal stimulation was performed. The effectiveness of the stimulation was evaluated by measuring the EEP response on the visual cortex. An individual peak in the EEP as a result of the retinal stimulation was observed. The stimulus function of the fabricated device operated normally when implanted into living body tissue. The promising application of the device as a retinal prosthesis was demonstrated. Although this Letter only reports the demonstration of the stimulus function of the device, the device also has a function to measure the electric potential of neural activity. Moreover, the device architecture has a flexible design, so a custom device can be designed for each application. For example, a large-size array of the order of several centimetres for electrocorticogram (ECoG) measurement or a brain stimulation electrode utilised to treat functional disorders of the brain can be fabricated easily.

Acknowledgment: A part of this study is the result of the 'Brain Machine Interface Development' carried out under the Strategic Research Program for Brain Sciences by the Ministry of Education, Culture, Sports, Science and Technology of Japan. All animal experiments were regulated with the animal experimentation guidelines at Nasa Institute of Science and Technology, Japan.

3 August 2012
doi: 10.1049/el.2012.2784

T. Noda, K. Sasagawa, T. Tokuda and J. Ohta (*Nara Institute of Science and Technology, Ikoma, Nasa 630-0192, Japan*)

E-mail: t-noda@ms.naist.jp

Y. Terasawa (*NIDEK Co., Ltd.*)

H. Tashiro (*Kyushu University*)

H. Kanda and T. Fujikado (*Osaka University*)

References

1 Chao, Z.C., Nagasaka, Y., and Fujii, N.: 'Long-term asynchronous decoding of arm motion using electrocorticographic signals in monkeys', *Front Neuroeng.*, 2010, **3**, (3), doi: 10.3389

2 Rubehn, B., Bosman, C., Oostenveld, R., Fries, P., and Stieglitz, T.: 'A MEMS-based flexible multichannel ECoG-electrode array', *J. Neural Eng.*, 2009, **6**, (3), p. 036003

3 Wise, K.D., and Najafi, K.: 'Microfabrication techniques for integrated sensors and microsystems', *Science*, 1991, **254**, (5036), pp. 1335–1342

4 Campbell, P.K., Jones, K.E., Huber, R.J., Horch, K.W., and Normann, R.A.: 'A silicon-based, three-dimensional neural interface: manufacturing processes for an intracortical electrode array', *IEEE Trans. Biomed. Eng.*, 1991, **38**, (8), pp. 758–768

5 Ohta, J., Yoshida, N., Kagawa, K., and Nunoshita, M.: 'Proposal of application of pulsed vision chip for retinal prosthesis', *Jpn. J. Appl. Phys.*, 2002, **41**, pp. 2322–2325

6 Tokuda, T., Hiyama, K., Sawamura, S., Sasagawa, S., Terasawa, Y., Nishida, K., Kitaguchi, Y., Fujikado, T., Tano, Y., and Ohta, J.: 'CMOS-based multichip networked flexible retinal stimulator designed for image-based retinal prosthesis', *IEEE Trans. Electron Devices*, 2009, **56**, (11), pp. 2577–2585

7 Kanda, H., Morimoto, T., Fujikado, T., Tano, Y., Fukuda, Y., and Sawai, H.: 'Electrophysiological studies of the feasibility of suprachoroidal-transretinal stimulation for artificial vision in normal and RCS rats', *Invest. Ophthal. Vis. Sci.*, 2004, **45**, (2), pp. 560–566

8 Fujikado, T., Morimoto, T., Kanda, H., Kusaka, S., Nakauchi, K., Ozawa, M., Matsushita, K., Sakaguchi, H., Ikuno, Y., Kamei, M., and Tano, Y.: 'Evaluation of phosphenes elicited by extraocular stimulation in normals and by suprachoroidal-transretinal stimulation in patients with retinitis pigmentosa', *Graefes Arch. Clin. Exp. Ophthalmol.*, 2007, **245**, (10), pp. 1411–1419